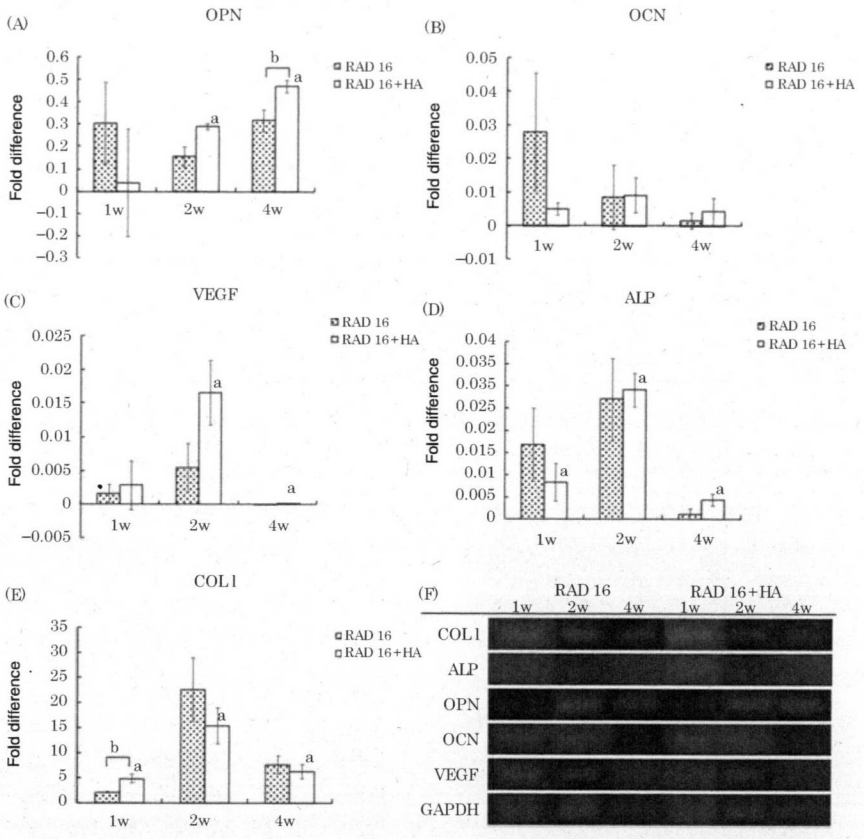

Figure 7. Osteogenic gene expression in the implants. Representative curves of mRNA levels of OPN (A), OCN (B), VEGF (C), ALP (D), and COL I (E) in each group are calculated by the 2::Ct formula. Experiment values are each expressed as the mean ± SD (n = 4). a: Statistically significant difference compared in the same group (p5 **0.05**). b: Statistically significant difference compared to all other groups (p5 0.05). Gel electrophoresis (F) show different gene expression levels corresponding to the quantitative analysis at different time points.

a peak level at 2 weeks; particularly, the VEGF gene in the RAD16 + HA group indicated the higher expression at that time point (Figure 7(C)). On the other hand, OPN gene expression increased during the period (Figure 7(A)), and, like the OCN gene, it likely had not yet been stimulated by 4 weeks, although the gene expression levels of the RAD16 + HA group ranged widely at 1 week (Figure 7(B)). Gel electrophoresis (Figure 7(F)) represented different gene expression levels corresponding to the quantitative analysis at different time points.

+ [Ver: 8.0r/W] [23.11.2009-5:35pm] [1-22] [Page No. 16] FIRST PROOFS {SICE_HP}JBA/JBA_356283.3d (jba) Paper: JBA_356328 Keyword

DISCUSSION

Many studies have demonstrated the feasibility of osteogenesis using atelocollagen as a reservoir for cell/tissue engineering in culture-based studies and transplantations in animal subjects [27–36]. Recently, novel hydrogels called self-assembling peptide matrices, have also been developed for 3D osteoblast proliferation and differentiation, mostly in *in* vitro studies [9,20,37–39]; however, fewer investigations have been published with respect to in vivo transplantation of these matrices, which we suspect might be the result of absorption of the self-assembling peptides when produced in animal bodies. Therefore, the present study describes the first use of a novel hydrogel, RAD16, for osteogenesis in an animal model. RAD16 possesses unique features as a tissue engineering material, where the peptide scaffold spontaneously self-assembles into nanofibers with 10–20 nm diameter. These nanofibers are highly hydrated, trapping water at a total volume content of 99.5%. Such a nanofiber scaffold preferably embeds cells in a 3D environment [40].

In the first part of this study, RAD16 containing two types of differently cultured cells was compared with embedded atelocollagen in cells under the same conditions. As demonstrated in a previous report [20], the present study similarly demonstrated that RAD16 (RO group) likely stimulated cell proliferation after incubation with the osteogenic supplements at the early time point of 1 day, whereas the other combinations showed a tendency to elevate cell proliferation gradually up to 2 weeks. Since cell proliferation at day 1 was represented, the cell numbers of all groups were increased up to approximately 10 times as many as the initially prepared number; therefore, the cells might be suggested at least viable in the given materials. Although it is well known that doses of dexamethasone appropriate for osteogenesis in cell culture are not suitable for cell proliferation, a RAD16 matrix cocultured in the osteogenic medium (***RO*** group) quickly accelerated the cell count but turned inhibitory by week 2. This strong stimulatory effect of RAD16 might be due in part to an unknown synergy between dexamethasone and the amino acid residual sequence environment of RAD16, with RGD peptides providing a suitable biological promotion for cells to attach and proliferate. Since the designated culture period in this study was only up to 2 weeks, mineralized nodules were not detected in all samples by staining technique (data not shown). However, RAD16, as well as atelocollagen in the osteogenic medium (RO and AO groups), stimulated ALP activity at 2 weeks (which was delayed a week relative to cell proliferation) while the other combinations (RN and AN groups) showed flat or declining activities during the same time (which was consistent

with its transcriptional change in mRNA). Recent studies have demonstrated a low capability of atelocollagen to elicit the osteogenic potential of the bone marrow MSCs treated with a nonosteogenic medium both *in* vitro [31] and in vivo [33–36], presenting no or less bone-related molecular cascade and no bony tissue regeneration, respectively. However, these studies also demonstrated osteogenesis when the cells were treated with the osteogenic supplements. The gene expressions examined in the present study resembled such expression profiles, except for COL I in the atelocollagen groups (AO and *AN gr*oups) at 2 weeks. On the other hand, RAD16 expressed the tested genes in excess in treatment of osteogenesis (RO) at 2 weeks; furthermore, COL I, ALP, and OPN genes were stimulated even in the normal medium without dexamethasone during the experimental period in our model. Hamada et al. [9] described ALP gene expression in the bone marrow MSCs hosted by RAD16 only with dexamethasone treatment; no expression was reported without dexamethasone. The difference between their experimental design and ours was the passages of the subculture of the primary MSCs after the cells were encapsulated in RAD16 following derivation from 6- or 7-week-old animals. Hence, cells cultured in the osteogenic condition for a longer period might have affected osteogenic activation in the 3D matrix.

From the results of the cocultured RAD16, it was significant that RAD16 incubated in the osteogenic medium induced the cells trapped inside to express osteogenic signals. We then hypothesized that RAD16 might be modified to serve as an implant matrix for cell-based tissue regeneration, assuming that the physiological issue of the rapid shrinkage of the hydrogel, generally observed in vivo, could be overcome with a Teflon pass-through socket accordingly provided to hold the RAD16 composite. As far as the specimens were sampled dealt on histology, they did not look so much minimized as had been expected to be, whereas RAD16 nakedly delivered in vivo was hardly maintained in its initial shape (data not shown). Recently, many studies have demonstrated enhancement of osteogenic indication in atelocollagen conjugated with porous HA or HA cement when such hydrogels were implanted in bony defects or intramuscular regions [32,33,41]. Additionally, RAD16 mixtures with HA particles induced the cocultured MSCs to be more osteogenic *in* vitro [37], on the other hand, the cocultured cells were unable to be identified from endogenous cells once implanted in our model because they had not been labeled; however, orchestrated cells all together were stimulated in terms of osteogenesis even postimplantation. In the present study, RAD16 was demonstrated of feasibility as an extracellular matrix at least within the examined

+ [Ver: 8.07r/W] [23.11.2009-5:35pm] [1-22] [Page No. 18] HIST ROES {SICE_FP_JBA_BA_356383} (jba) Paper: JBA_356328 Keyword

periods although a positive control such as atelocollagen was not provided for the implant application. It must be taken into account in our next study that RAD16, an implant carrier, be compared with widely used substances such as atelocollagen.

In summary, our animal study supports the potential of RAD16 as an osteogenic substrate, in which bone-related genes such as COL I, ALP, and OPN with VEGF, which are often referred as early markers of bone generation, were well-activated by 2 weeks postimplantation. Localization of OPN mRNA was restricted to the hydrogel surface, and cells aligned on the HA particles also had a weak but positive signal for OPN mRNA. However, mineralized nodules were detected in neither RAD16 alone nor RAD16 with HA particles within the study periods, which were followed by less expression of OCN mRNA and its unidentified localization. It has been suggested and noted that a local source of calcium could be attributed to HA particles scattered in the RAD16 matrix [37], therefore, the amount of HA provided in the hydrogel might not have been enough to promote osteogenic differentiation of MSCs in our study. Conversely, the study period of 4 weeks might have been too short to bring about mineral apposition; nevertheless, positive signs of osteogenesis were perceived in the RAD16-supported implants. In view of these results, RAD16 might be thoroughly considered as a candidate to be an attractive molecule for manufacturing biomaterials.

CONCLUSION

We investigated a possible use of RAD16 as a biocompatible material for bone formation. The RAD16 matrices used in this study showed osteogenic differentiation of bone marrow derived from MSCs and cocultured within the hydrogel, but no newly formed bone was generated. Thus, continued investigation of RAD16 as a useful material for tissue engineering is clearly warranted.

ACKNOWLEDGMENTS

We sincerely thank Dr Keiichi Ohya and Dr Hitoyata Shimokawa, Pharmacology, Tokyo Medical and Dental University, and Dr Michiko Suzuki, Oral Implantology and Regenerative Dental Medicine, Tokyo Medical and Dental University, for technical help and advice. This research was supported by a grant from the Japan Society for the Promotion of Science (No. # 17689059,19390513) and a grant from the Center of Excellence Program for Frontier Research on Molecular Destruction and Reconstruction of Tooth and Bone at Tokyo Medical and Dental University.

REFERENCES

1. Khan, S.N., Cammisa, F.P., Sandha, H.S., Diwan, A.D., Girardi, F.P. and Lane, J.M. The Biology of Bone Grafting, J. Am. Acad. Orthopaed. Surg., 2005: 13: 77–86.
2. Derubeis, A.R. and Cancedda, R. Bone Marrow Stromal Cells (BMSCs) in Bone Engineering: Limitations and Recent Advances, Ann. Biomed. Eng., 2004: 32: 160–165.
3. Mistry, A.S. and Mikos, A.G. (2005). Tissue Engineering Strategies for Bone Regeneration, Regenerative Medicine Ii: Clinical and Preclinical Applications, New York, Springer.
4. Ohgushi, H. and Caplan, A.I. Stem Cell Technology and Bioceramics: From Cell to Gene Engineering, J. Biomed. Mater. Res., 1999: 48: 913–927.
5. Tuan, R.S., Boland, G. and Tuli, R. Adult Mesenchymal Stem Cells and Cell-based Tissue Engineering, Arthritis Res. Ther., 2003: 5: 32–45.
6. Maniatopoulos, C., Sodek, J. and Melcher, A.H. Bone-formation In Vitro by Stromal Cells Obtained from Bone-marrow of Young-adult Rats, Cell Tissue Res., 1988: 254: 317–330.
7. Cen, L., Liu, W., Cui, L., Zhang, W.J. and Cao Y.L. Collagen Tissue Engineering: Development of Novel Biomaterials and Applications, Pediatr. Res., 2008: 63: 492–496.
8. Choumerianou, D.M., Dimitriou, H. and Kalmanti, M. Stem cells: Promises Versus Limitations, Tissue Eng. Part B: Rev., 2008: 14: 53–60.
9. Hamada, K., Hirose, M., Yamashita, T. and Ohgushil, H. Spatial Distribution of Mineralized Bone Matrix Produced by Marrow Mesenchymal Stem Cells in Self-assembling Peptide Hydrogel Scaffold, J. Biomed. Mater. Res. Part A, 2008: 84: 128–136.
10. Zhou, Y.F., Chen, F.L., Ho, S.T., Woodruff, M.A., Lim, T.M. and Hutmacher, D.W. Combined Marrow Stromal Cell-sheet Techniques and High-strength Biodegradable Composite Scaffolds for Engineered Functional Bone Grafts, Biomaterials, 2007: 28: 814–824.
11. Zhang, S.G., Holmes, T.C., Dipersio, C.M., Hynes, R.O., Su, X. and Rich, A. Self-complementary Oligopeptide Matrices Support Mammalian-cell Attachment, Biomaterials, 1995: 16: 1385–1393.
12. Holmes, T.C. Novel Peptide-based Biomaterial Scaffolds for Tissue Engineering, Trends Biotechnol., 2002: 20: 16–21.
13. Zhao, X.J. and Zhang, S.G. Fabrication of Molecular Materials Using Peptide Construction Motifs, Trends Biotechnol., 2004: 22: 470–476.
14. Zhang, S.G., Holmes, T., Lockshin, C. and Rich, A. Spontaneous Assembly of a Self-complementary Oligopeptide to Form a Stable Macroscopic Membrane, Proc. Natl Acad. Sci. USA, 1993: 90: 3334–3338.
15. Kisiday, J., Jin, M., Kurz, B., et al. Self-assembling Peptide Hydrogel Fosters Chondrocyte Extracellular Matrix Production and Cell Division: Implications for Cartilage Tissue Repair, Proc. Natl Acad. Sci. USA, 2002: 99: 9996–10001.
16. Semino, C.E., Merok, J.R., Crane, G.G., Panagiotakos, G. and Zhang, S.G. Functional Differentiation of Hepatocyte-like Spheroid Structures from

Putative Liver Progenitor Cells in Three-dimensional Peptide Scaffolds, Differentiation, 2003: 71: 262–270.

17. Spencer, N.J., Cotanche, D.A. and Klapperich, C.M. Peptide- and Collagen-based Hydrogel Substrates for In Vitro Culture of Chick Cochleae, Biomaterials, 2008: 29: 1028–1042.

4 18. Tanaka, T. Bone Augmentation by Bone Marrow Mesenchymal Stem Cells Cultured in Three-dimensional Biodegradable Polymer Scaffolds, J. Biomed. Mater. Res. Part A, 2008.

19. Wang, S., Nagrath, D., Chen, P.C., Berthiaume, F. and Yarmush, M.L. Three-dimensional Primary Hepatocyte Culture in Synthetic Self-assembling Peptide Hydrogel, Tissue Eng Part A, 2008: 14: 227–236.

20. Bokhari, M.A., Akay, G., Zhang, S.G. and Birch, M.A. Enhancement of Osteoblast Growth and Differentiation In Vitro on a Peptide Hydrogel - polyHIPE Polymer Hybrid Material, Biomaterials, 2005: 26: 5198–5208.

21. Misawa, H., Kobayashi, N., Soto-Gutierrez, A., et al. PuraMatrix (TM) Facilitates Bone Regeneration in Bone Defects of Calvaria in Mice, Cell Transplant, 2006: 15: 903–910.

22. Flautre, B., Anselme, K., Delecourt, C., Lu, J., Hardouin, P. and Descamps, M. Histological Aspects in Bone Regeneration of an Association with Porous Hydroxyapatite and Bone Marrow Cells, J. Mater. Sci. Mat. Med., 1999: 10: 811–814.

23. Kurashina, K., Kurita, H., Takeuchi, H., Hirano, M., Klein, C. and Degroot, K. Osteogenesis in Muscle with Composite Graft of Hydroxyapatite and Autogenous Calvarial Periosteum - A Preliminary Report, Biomaterials, 1995: 16: 119–123.

24. Ripamonti, U. Osteoinduction in Porous Hydroxyapatite Implanted in Heterotopic Sites of Different Animal Models, Biomaterials, 1996: 17: 31–35.

25. Yoshikawa, T., Ohgushi, H., Akahane, M., Tamai, S. and Ichijima, K. Analysis of Gene Expression in Osteogenic Cultured Marrow Hydroxyapatite Construct Implanted at Ectopic Sites: A Comparison with the Osteogenic Ability of Cancellous Bone, J. Biomed. Mater. Res., 1998: 41: 568–573.

26. Yoshikawa, T., Ohgushi, H. and Tamai, S. Immediate Bone Forming Capability of Prefabricated Osteogenic Hydroxyapatite, J. Biomed. Mater. Res., 1996: 32: 481–492.

27. Yamazoe, K., Mishima, H., Torigoe K., et al. Effects of Atelocollagen Gel Containing Bone Marrow-Derived Stromal Cells on Repair of Osteochondral Defect in a Dog, J. Vet. Med. Sci., 2007: 69: 835–839.

28. Hisatome, T., Yasunaga, Y., Yanada, S., Tabata, Y., Ikada, Y. and Ochi, M. Neovascularization and Bone Regeneration by Implantation of Autologous Bone Marrow Mononuclear Cells, Biomaterials, 2005: 26: 4550–4556.

29. Yoshida, K., Bessho, K., Fujimura, K., et al. Enhancement by Recombinant Human Bone Morphogenetic Protein-2 of Bone Formation by Means of Porous Hydroxyapatite in Mandibular Bone Defects, J. Dent. Res., 1999: 78: 1505–1510.

30. Hasegawa, N., Kawaguchi, H., Hirachi, A., et al. Behavior of Transplanted Bone Marrow-Derived Mesenchymal Stem Cells in Periodontal Defects, ***J. Periodontol.***, 2006: 77: 1003–1007.

31. Ikeuchi, M., Dohi, Y., Horiuchi, K., et al. Recombinant Human Bone Morphogenetic Protein-2 Promotes Osteogenesis Within Atelopeptide Type I Collagen Solution by Combination with Rat Cultured Marrow Cells, J. Biomed. Mater. Res., 2002: 60: 61–69.

32. Du, C., Cui, F.Z., Feng, Q.L., Zhu, X.D. and de Groot, K. Tissue Response to Nano-Hydroxyapatite/Collagen Composite Implants in Marrow Cavity, J. Biomed. Mater. Res., 1998: 42: 540–548.

33. Kusumoto, K., Bessho, K., Fujimura, K., Ogawa, Y. and Iizuka, T. Intramuscular Osteoinduction and Bone Marrow Formation by the Implantation of rhBMP-2 with Atelopeptide Type I Collagen, Br. J. Oral ***Maxillofac. Surg.***, 1997: 35: 433–437.

34. Kusumoto, K., Bessho, K., Fujimura, K., Konishi, Y., Ogawa, Y. and Iizuka, T. Self-Regenerating Bone Implant: Ectopic Osteoinduction Following Intramuscular Implantation of a Combination of rhBMP-2, Atelopeptide Type I Collagen and Porous Hydroxyapatite, J. Craniomaxillofac. Surg., 1996: 24: 360–365.

35. Nakagawa, T. and Tagawa, T. Ultrastructural Study of Direct Bone Formation Induced by BMPs-Collagen Complex Implanted into an Ectopic Site, ***Oral*** Dis., 2000: 6: 172–179.

36. Hou, L.T., Liu, C.M., Liu, B.Y., et al. Tissue Engineering Bone Formation in Novel Recombinant Human Bone Morphogenic Protein 2-Atelocollagen Composite Scaffolds, ***J. Periodontol.***, 2007: 78: 335–343.

37. Garreta, E., Gasset, D., Semino, C. and Borros, S. Fabrication of a Three-dimensional Nanostructured Biomaterial for Tissue Engineering of Bone, Biomol. Eng., 2007: 24: 75–80.

38. Shirai, K., Ishisaki, A., Kaku, T., Tamura, M. and Furuichi, Y. Multipotency of Clonal Cells Derived from Swine Periodontal Ligament and Differential Regulation by Fibroblast Growth Factor and Bone Morphogenetic Protein, J. Periodontal. Res., 2009: 44: 238–247.

39. Horii, A., Wang, X., Gelain, F. and Zhang, S. Biological Designer Self-Assembling Peptide Nanofiber Scaffolds Significantly Enhance Osteoblast Proliferation, Differentiation and 3-D Migration, ***PLoS*** ONE, 2007: 2: e190.

40. Semino, C.E., Merok, J.R., Crane, G.G., Panagiotakos, G. and Zhang, S. Functional Differentiation of Hepatocyte-like Spheroid Structures from Putative Liver Progenitor Cells in Three-dimensional Peptide Scaffolds, ***Differentiation***, 2003: 71: 262–270.

41. Takechi, M., Miyamoto, Y., Ishikawas, K., et al. Histological Evaluation of Apatite Cement Containing Atelocollagen, ***Dent. Mater.*** J., 2007: 26: 194–200.

Molecular and Tissue Responses in the Healing of Rat Calvarial Defects After Local Application of Simvastatin Combined With Alpha Tricalcium Phosphate

Myat Nyan,[1,2,3] Takayuki Miyahara,[1,2] Kanako Noritake,[1,2] Jia Hao,[1,2] Reena Rodriguez,[1,2] Shinji Kuroda,[1] Shohei Kasugai[1,2]

[1] Department of Oral Implantology and Regenerative Dental Medicine, Tokyo Medical and Dental University, Tokyo, Japan

[2] Global Center of Excellence Program, International Research Center for Molecular Science in Tooth and Bone Diseases, Tokyo Medical and Dental University, Tokyo, Japan

[3] Department of Prosthodontics, University of Dental Medicine, Yangon, Myanmar

Received 29 May 2009; revised 20 August 2009; accepted 27 September 2009
Published online 18 December 2009 in Wiley InterScience (www.interscience.wiley.com). DOI: 10.1002/jbm.b.31559

Abstract: We have previously reported that healing of rat calvarial defects was enhanced by application of alpha tricalcium phosphate (αTCP) combined with simvastatin, a cholesterol synthesis inhibitor. The purpose of the present study was to investigate the cellular and molecular mechanisms in this phenomenon. Rat calvarial defects were grafted with αTCP with or without simvastatin or left untreated. Animals were sacrificed on 3, 7, 10, 14, and 21 days postoperatively and histological changes in the defect region were assessed. Gene expression patterns were examined by RT-PCR. Proliferation and migration of osteoprogenitor cells from the dura mater were increased in simvastatin group from day 3 to day 10 ($p < 0.01$). New bone formation was significantly increased in simvastatin group on day 14 and day 21 ($p < 0.01$). BMP-2 expression was significantly higher in simvastatin group on day 3 and day 14 ($p < 0.05$) and maintained until day 21. Increased upregulation of TGF-β1 was also observed in the simvastatin group on day 7 ($p < 0.05$) which was maintained until day 14. These findings suggest that the proliferation and recruitment of osteoprogenitor cells were critical steps in early stage of bone healing and that these steps were enhanced by TGF-β1 and BMP-2, which were stimulated by simvastatin. © 2009 Wiley Periodicals, Inc. J Biomed Mater Res Part B: Appl Biomater 93B: 65–73, 2010

Keywords: bone healing; simvastatin; alpha tricalcium phosphate; BMP-2; TGF-β; bone formation

INTRODUCTION

For regeneration of defective or lost bone tissue, various techniques for tissue engineering have been introduced. *In situ* bone regeneration therapy is one of them in which osteoconductive scaffolds combined with bioactive molecules are applied to stimulate the local host cells to upregulate osteoblastic differentiation and subsequent bone formation. Bone morphogenetic proteins (BMPs) are promising candidates for this approach of tissue engineering; however, there are still some problems to be solved for clinical application.[1] Simvastatin is one of the most commonly prescribed cholesterol lowering drugs, which has been shown to stimulate expression of BMP-2 *in vitro* and promote bone formation *in vivo*.[2] Recently, many research works have been emphasized on the local application of statins for *in situ* bone regeneration and repair.[3–16] We have also reported in our previous study that optimal dose of simvastatin combined with alpha tricalcium phosphate (αTCP) stimulated bone regeneration in the calvarial osteotomy defects in rats.[17] The objective of the present study was to investigate the molecular and cellular mechanisms in the early stage of bone healing by the application of simvastatin-αTCP combination in the rat calvarial defects.

MATERIALS AND METHODS

Sample Preparation and Measurement of *In Vitro* Drug Release

αTCP particles (Advance Co., Tokyo, Japan) having 500–700 μm in diameter and porous structure (mean pore size

Correspondence to: M. Nyan (e-mail: myatnyan@gmail.com)
Contract grant sponsors: Global Center of Excellence Program, International Research Center for Molecular Science in Tooth and Bone Diseases, Tokyo Medical and Dental University, Tokyo, Japan

~5 μm, mean porosity ~27%) were used. The samples were prepared according to the methods previously described.[17] Simvastatin (OHARA Pharmaceutical Co. Ltd., Koka, Shiga, Japan) was dissolved in ethanol and the solution was applied to the αTCP particles by dropping under sterile conditions. Ethanol was dried out completely in a laminar flow hood. Each sample was composed of 0.1 mg simvastatin combined with 14 mg αTCP particles. This dose was determined as the optimal dose for combining with αTCP to stimulate bone regeneration in the previous study. The loading efficacy was determined by dividing the retained amount of simvastatin by the initial loaded simvastatin concentration multiplied by 100%.

The release of simvastatin was measured using a UV-Visible spectrophotometer, Nanodrop, ND-1000 (NanoDrop Technologies, Wilmington). The spectrometer was calibrated using 6 standards of simvastatin solution at 37°C. The absorbance was measured at 238 nm and working curve for calculation of simvastatin concentrations was established from the absorbance values. The samples were placed in 500 μL of 0.1*M* tris buffer solution (pH 7.4), and positioned in an Taitec Personal 11 Shaker (Taitec Corp., Tokyo, Japan) set at 100 rpm and 37°C. The amount of drug released into the tris buffer was measured 24 hr after the initial immersion, then every day for 14 days. The cumulative concentration was calculated using the previously determined working curve.

Animal Procedures

The animal experiment protocol was approved by the institutional committee for animal experiments. Bilateral parietal bone defects were created according to the method previously reported. Male Wistar rats (16 weeks old) were anesthetized with a combination of ketamine-xylazine (40 and 5 mg/kg). The dorsal part of the cranium was shaved and prepared aseptically for surgery. A 20-mm long incision in the scalp along the sagittal suture was made, and the skin, subcutaneous tissue and periosteum were reflected, exposing the parietal bones. Two full-thickness bone defects of 5 mm diameter were trephined in the dorsal part of the parietal bone lateral to the sagittal suture. A 5-mm trephine bur was used to create the defects under constant irrigation with sterile physiologic solution to prevent overheating of the bone edges. Care was taken during the surgical procedure to prevent damage to dura mater. In TCP group, each defect was filled with 14 mg of αTCP (30 rats) and in simvastatin group, with 14 mg of simvastatin-αTCP combination (30 rats). In 30 animals, both defects were left unfilled to serve as control group.

Histological Observation

For histological observations, three rats from each group were sacrificed at 3, 7, 10, 14, and 21 days after surgery. The specimens were fixed in 10% neutralized formalin for 1 week, decalcified in EDTA for 4 weeks, and then embedded in paraffin. Coronal sections of about 5 μm thickness were cut, stained with haematoxylin-eosin and observed under an optical microscope (Biozero, Keyence, Tokyo, Japan). The image analysis was performed by using a computer-based image analyzing software (Image J, NIH) to measure the cell density and to quantify the newly formed bone area within the defect. The cell counter tool in the Image J software was applied to count the number of osteoprogenitor-like cells by clicking on the image of each cell manually after these cells were visually determined according to their morphology. The cell counter tool marked the counted cells so that repeated counting was avoided. The bone fill percentage (%) was calculated from the values of total defect area and area of newly formed bone.

Real-Time PCR Analysis

For gene expression analysis, three rats from each group were sacrificed at 3, 7, 10, 14, and 21 days after surgery. Two bone samples incorporating the individual defect region were obtained from parietal bones of each rat. Total RNA was extracted from the bone samples by using Trizol Reagent (Invitrogen, Carlsbad, CA). Complementary DNAs (cDNAs) were synthesized using a commercial kit (Superscript III First-Strand Synthesis Supermix, Invitrogen) according to the manufacturer's recommendations. Oligonucleotide primers were designed for amplification of messenger RNA (mRNA) encoding the following genes: ratGAPDH (forward: 5′-AACTCCCATTCTTCCACCTT-3′, reverse: 3′AGGGCCTCTCTCTTGCTCT-5′), ratBMP-2 (forward: 5′-AAGGCACCCTTTGTATGTGG-3′, reverse: 3′-CATGCCTTAGGGATTTTGGA-5′), ratTGF-beta1 (forward: 5′-CAACAATTCCTGGCGTTACC-3′, reverse: 3′-TGGGACTGATCCCATTGATT-5′) and ratVEGF (forward: 5′-TTGAGACCCTGGTGGACATC-3′, reverse: 3′-CTCCT-ATGTGCTGGCTTTGG-5′).

Real-time PCR quantification was performed with SYBR green PCR master-mix (Applied Biosystems) on an Applied Biosystems 7300 Real Time PCR System (ABI, Foster City, CA). Expression levels were determined using the relative threshold cycle (C_T) method as described by the manufacturer of the detection system. Expression levels were stated in terms of fold increase or decrease relative to un-operated normal rats of the same age. This was calculated for each gene by evaluating the expression $2^{-\Delta\Delta C_T}$, where $\Delta\Delta C_T$ is the result of subtracting $[C_{T\text{gene}} - C_{T\text{GAPDH}}]_{(\text{unoperated calibrator})}$ from $[C_{T\text{gene}} - C_{T\text{GAPDH}}]_{(\text{experimental group})}$.

Statistical Analysis

Data were firstly analyzed by one-way ANOVA. When this analysis suggested a significant difference between groups ($p < 0.05$), the data were further analyzed by Tukey *post hoc* multiple comparison tests.

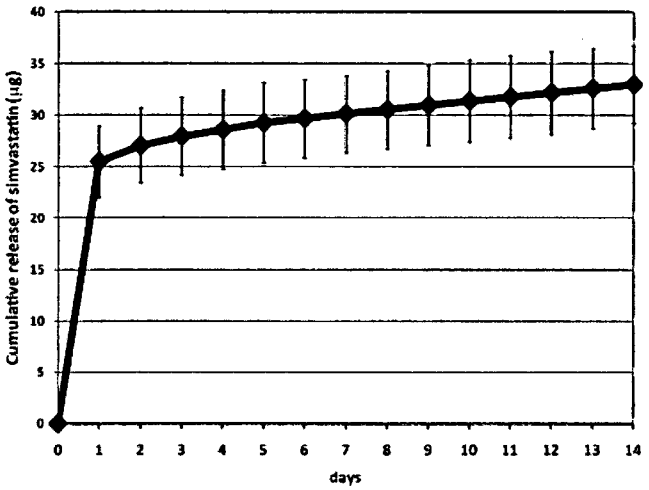

Figure 1. *In vitro* release pattern of simvastatin from αTCP. Values were shown as mean ± SD, $n = 5$.

RESULTS

In Vitro Release Behavior of Simvastatin From Alpha-Tricalcium Phosphate

The observed drug loading efficacy of αTCP for simvastatin was 93.4 ± 5.8%. Approximately 25% of adsorbed simvastatin was released after 24 hr. This initial burst release was followed by the gradual and stable release of the drug that was maintained until 2 weeks (Figure 1).

Histological Features

At day 3 after surgery, a significant thickening of dura mater was observed in simvastatin- αTCP combination group at the bone edges as well as in the middle of the defect. Round or cuboidal cells resembling undifferentiated mesenchymal cells and some osteoprogenitor-like cells migrated from dura mater to the area between the αTCP particles and dura mater. Some of these cells were also observed in the pores at the periphery of the particles which were located adjacent to the dura mater surface [Figure 2(c)]. On the other hand, control group showed the proliferation and migration of bone marrow mesenchymal cells from the bone edges and osteogenic cells from the periosteum over the bone edges. The middle of the defect was filled with connective tissue. Both control group and TCP group showed less extent of dura mater thickening and cell migration than simvastatin-αTCP combination group [Figure 2(a,b)].

At day 7, cell density became increased associated with formation of blood vessels in all groups. The cellular migration became more extensive in simvastatin-αTCP combination group at the center of the defect as well as near the bone edges. These cells took the morphology of proliferating preosteoblasts and recruited between αTCP particles and in the space between αTCP and bone edges. In some places, the cells resembling active osteoblasts condensed and began to lay down bone matrix [Figure 3(c,d)]. In the control group, the cellular proliferation was seen only at the bone edges whereas TCP group showed cell migration from dura mater at the middle of defect [Figure 3(a,b)].

At day 10, the osteogenic cells recruited between the TCP particles resembling preosteoblasts continued proliferation and migrating around the periphery of TCP particles. Some of these cells became differentiated into osteoblasts and began to lay down bone matrix in the simvastatin-αTCP combination group [Figure 4(c,d)]. Cell migration continued into the inner portion of TCP particles in both TCP and simvastatin-αTCP combination groups while many blood vessels were formed around the TCP particles [Figure 4(b,c)]. In the control group, the recruited cells at the bone edges differentiated into osteoblasts and began to form new bone [Figure 4(a)]. Cellular migration and proliferation were significantly higher in simvastatin-αTCP combination group at day 3 to day 10 ($p < 0.01$) (Figure 5).

At day 14, osteoblast differentiation and bone formation became extensive in the simvastatin-αTCP combination group so that the area between the αTCP particles became filled with newly formed bone. Active osteoblasts lined on this newly formed bone surface. The cells inside the αTCP particles also differentiated into osteoblasts and secreted bone matrix in this group [Figure 6(c)]. The cells recruited between αTCP particles in αTCP group also began to differentiate and synthesize bone matrix [Figure 6(b)]. In the control group, osteoblasts continued to form thin layer of new bone toward the center of the defect [Figure 6(a)].

At day 21, in simvastatin group, osteogenic cell migration and recruitment continued at many places eventually invading into the middle of the αTCP particles. New bone deposition was observed in the middle of the αTCP particles which were almost completely surrounded by the regenerated bone. Some parts of this new bone in contact with αTCP particles become mature and formed marrow spaces. New bone extensively replaced the αTCP particles which were located close to dura mater [Figure 7(c)]. In αTCP group, new bone was formed in the spaces between some particles but not as extensively as simvastatin group [Figure 7(b)]. In control group, osteoblasts lining along the newly formed bone surface became flattened and the center of the defect was filled with connective tissue [Figure 7(a)]. The percentage of new bone area was significantly higher in simvastatin-αTCP combination group at day 14 and day 21 ($p < 0.01$) (Figure 8).

Gene Expression Profiles

Gene expression experiments were conducted to investigate whether increased cellular proliferation and recruitment and augmented bone regeneration could be linked to TGF-β, BMP-2, and VEGF. All groups showed increased expression of TGF-β1 and BMP-2 from day 3 to 21. In simvastatin group, BMP-2 was upregulated since day 3 at a higher level than other groups ($p < 0.05$). All groups showed sim-

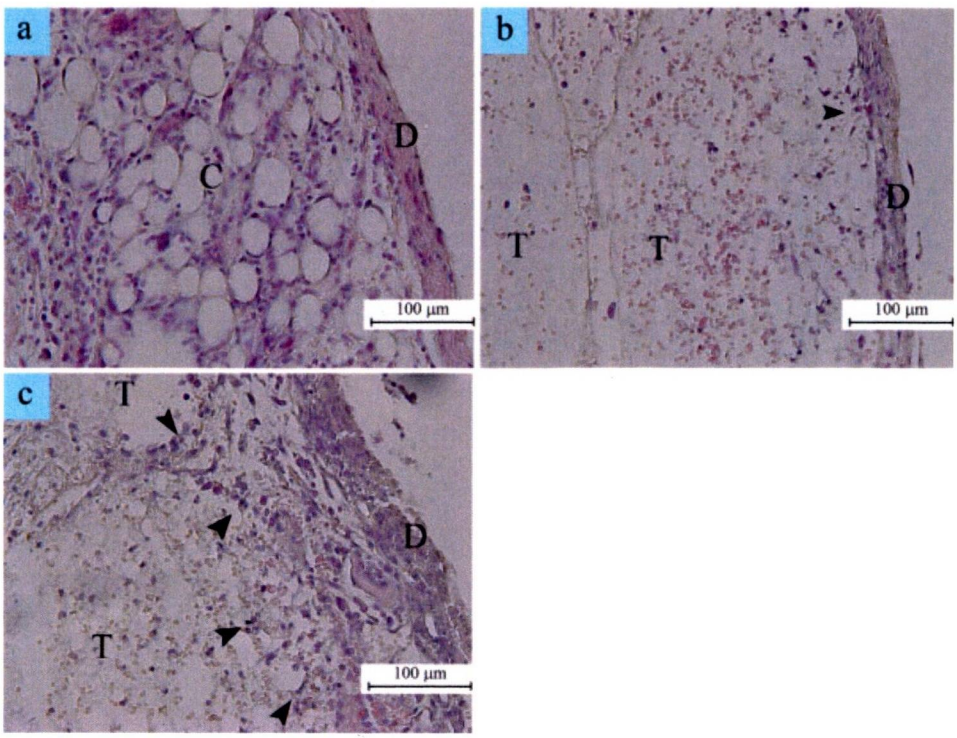

Figure 2. Photomicrographs of the calvarial defects at day 3 representing middle of the bone defects of (a) control (b) TCP and (c) simvastatin-αTCP combination groups. Arrow heads denote migrating osteogenic cells. D, dura mater; T, αTCP particles; C, connective tissue. [Color figure can be viewed in the online issue, which is available at www.interscience.wiley.com.]

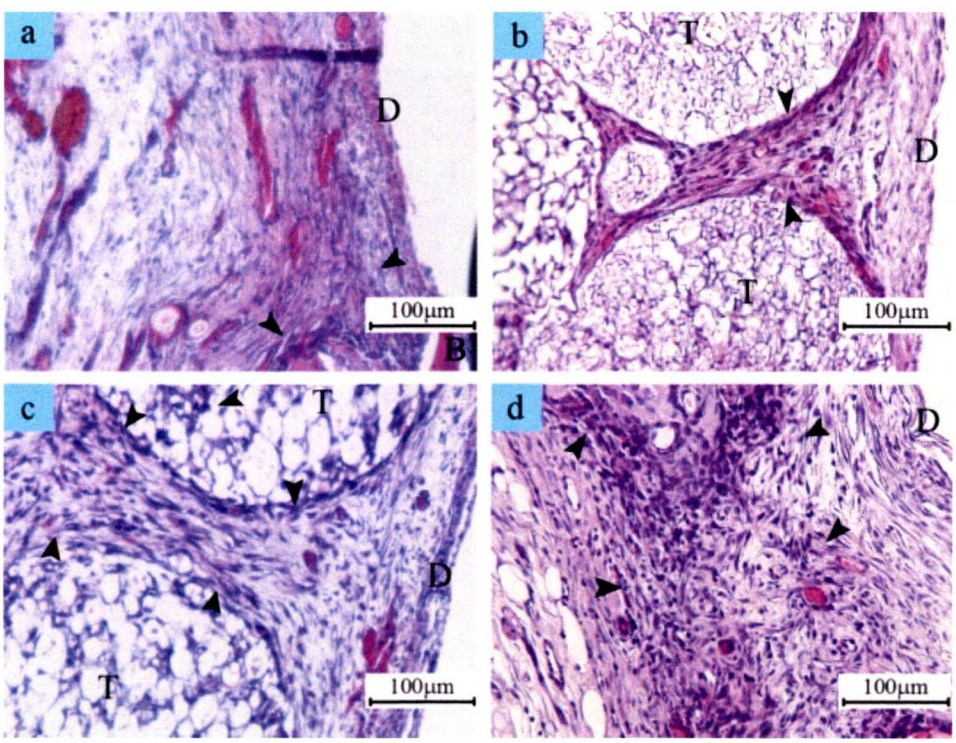

Figure 3. Photomicrographs of the calvarial defects at day 7 representing middle of the bone defects of (b) TCP and (c) simvastatin-αTCP combination groups. Panel (a) and (d) show control and simvastatin-αTCP combination groups near the bone edge. Arrow heads denote proliferating pre-osteoblasts. D, dura mater; T, αTCP particles; B, old bone. [Color figure can be viewed in the online issue, which is available at www.interscience.wiley.com.]

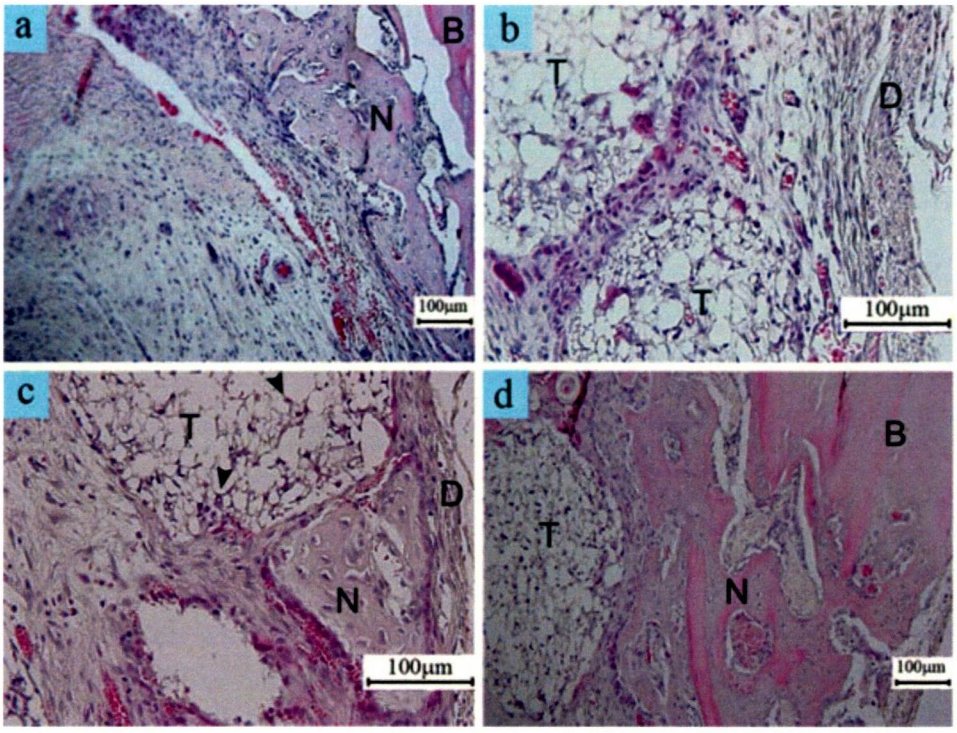

Figure 4. Photomicrographs of the calvarial defects at day 10 representing middle of the bone defects of (b) TCP and (c) simvastatin-αTCP combination groups. Panel (a) and (d) show control and simvastatin-αTCP combination groups near the bone edge. Arrow heads denote osteogenic cells migrating into αTCP particle. D, dura mater; T, αTCP particles; B, old bone; N, newly formed bone. [Color figure can be viewed in the online issue, which is available at www.interscience.wiley.com.]

ilar levels of BMP-2 mRNA expression at day 7 and day 10. The expression became higher again in simvastatin group at day 14 ($p < 0.05$) and maintained high expression until day 21.

All groups revealed slight increase in TGF-β1 expression at day 3. Then, from day 7 till day 21, the expression became increased in all groups. TGF-β1 expression was dramatically upregulated in simvastatin group at day 7 ($p < 0.05$) and maintained at higher levels until day 14. In contrast, VEGF mRNA expressions in all groups were increased at day 3 and day 7 compared with baseline (normal unoperated rats). At day 10 and 14, simvastatin group showed higher expressions of VEGF while expression levels in other groups tended to decrease toward the baseline level. However, the differences were not statistically significant. At day 21, all groups showed similar expression level (Figure 9).

DISCUSSION

Molecular and cellular mechanisms in the early healing of rat calvarial defects after local application of simvastatin-αTCP combination were examined in this study.

We found increased proliferation and migration of the osteogenic cells mainly from dura mater and also from bone edges in simvastatin group at the initial stage of healing (day 3, 7, and 10). During bone healing, the mesenchymal stem cells play an important role providing the osteogenic cells. The potential sources of stem cells are the bone marrow, the granulation tissue, the periosteum, the endosteum, and the surrounding soft tissues.[18,19] The dura mater is a component of the meninges, a group of fibrous connective tissues which function to protect both the brain and spinal cord.[20] Many studies have demonstrated that the initial patterning and subsequent regeneration of the cranial vault is regulated by secreted cytokines and donated precursor cells from the dura mater.[21–24]

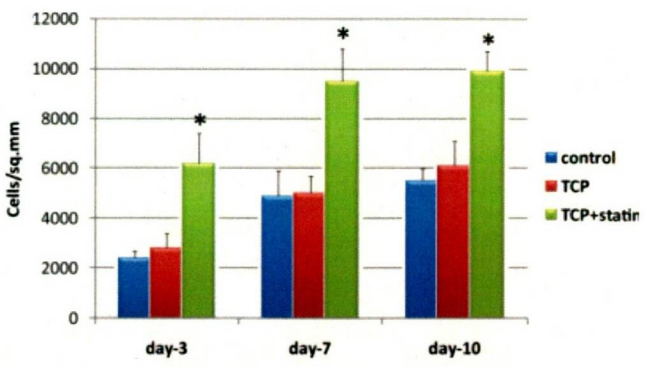

Figure 5. Cell density in the defect region at the middle of the bone defects of control, TCP and simvastatin-αTCP combination groups at day 3, 7, and 10. Values were shown as mean ± SD, $n = 6$. *$p < 0.01$ compared with control and TCP groups at corresponding time point. [Color figure can be viewed in the online issue, which is available at www.interscience.wiley.com.]

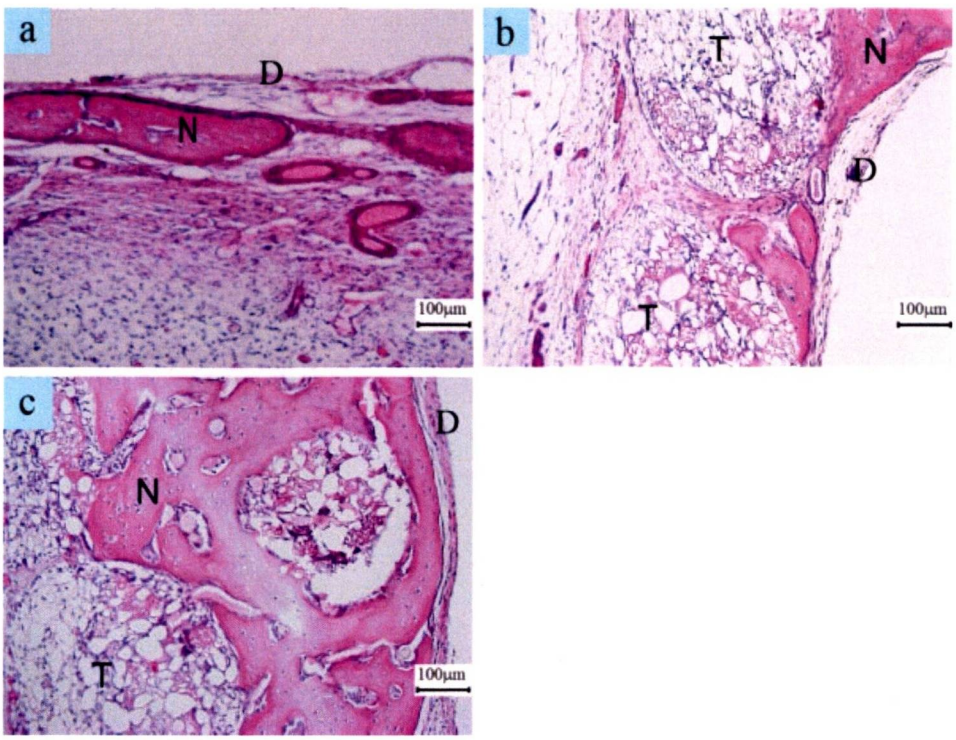

Figure 6. Photomicrographs of the calvarial defects at day 14 representing middle of the bone defects of (a) control (b) TCP and (c) simvastatin-αTCP combination groups. D, dura mater; T, αTCP particles; N, newly formed bone. [Color figure can be viewed in the online issue, which is available at www.interscience.wiley.com.]

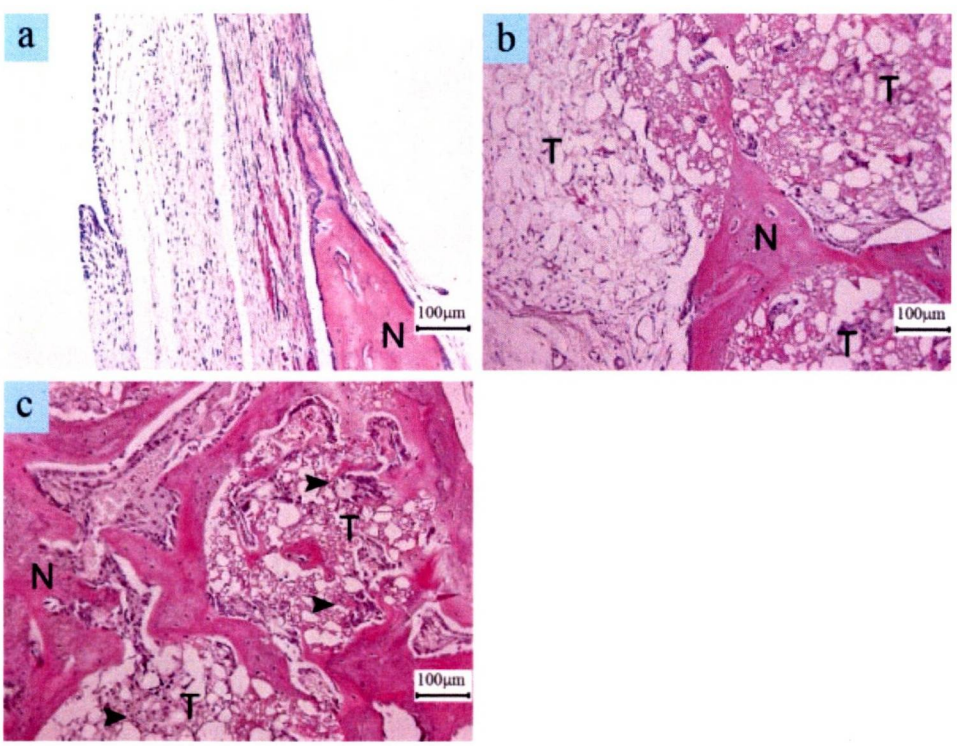

Figure 7. Photomicrographs of the calvarial defects at day 21 representing middle of the bone defects of (a) control (b) TCP and (c) simvastatin-αTCP combination groups. Arrow heads denote proliferating osteogenic cells. T, αTCP particles; N, newly formed bone. [Color figure can be viewed in the online issue, which is available at www.interscience.wiley.com.]

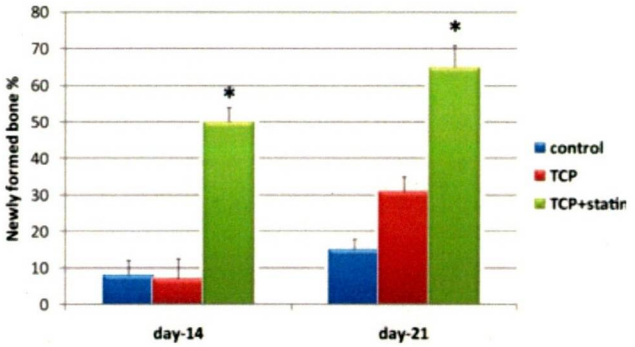

Figure 8. Comparison of new bone area between control, TCP, and simvastatin-αTCP combination groups at day 14 and day 21. Values were shown as mean ± SD, $n = 6$. *$p < 0.01$ compared with other groups at the same time point. [Color figure can be viewed in the online issue, which is available at www.interscience.wiley.com.]

The results of our *in vitro* experiment showed an initial burst release of simvastatin from αTCP. A similar pattern of release is expected in the bone defect and the released simvastatin would induce the dura mater for cytokine secretion and precursor cells stimulation at the initial phase of bone healing. This appears to be a critical step in the early stage of bone healing providing osteogenic cells which were recruited in the spaces between αTCP particles and between the particles and the dura mater by day 10.

Real-time PCR analysis revealed significantly augmented upregulation of BMP-2 at day 3 in simvastatin-αTCP combination group. It has been reported that BMP-2 stimulates chemotatic migration of mesenchymal progenitor cells and stromal osteoblasts.[25,26] Upregulation of BMP-2 at day 3 would be attributed to the initial migration and recruitment of osteogenic cells from dura mater in simvastatin-αTCP combination group. Transforming growth factor beta (TGF-β) is involved in fracture repair and it is produced by degranulated platelets after initial injury and also by osteoblasts and chondrocytes at later stages, which enhances the proliferation of these cells as well as that of mesenchymal cells and preosteoblasts.[27] TGF-β also appears to stimulate osteoblast proliferation, which presumably increases the pool of committed osteoblast precursors.[28,29] In addition, it has been shown to have strong osteoblast chemotatic effect.[30] In our experiment, TGF-β1 expression was highly upregulated in simvastatin-αTCP combination group at day 7, reaching peak at day 10 and maintained the high expressions until day 14. Histologically, extensive proliferation and migration of osteogenic cells were observed at day 7 and day 10, and continued, albeit to a less extent, at day 14 and day 21. These data suggest that TGF-β1 would play a role in early proliferation of osteogenic cells and continued proliferation and migration of osteoblasts in simvastatin-αTCP combination group.

At day 14, extensive differentiation of recruited cells to osteoblasts and active formation of new bone were evident in the simvastatin-αTCP combination group. Although pre-existing osteoblasts may be involved in the bone repair to some extent, the differentiation of pluripotential mesenchymal stem cells into osteoblasts and chondral cells is regarded as a critical step in the bone healing.[31] Expression of BMP-2 was upregulated significantly at day 14 and its expression was maintained until day 21 in simvastatin

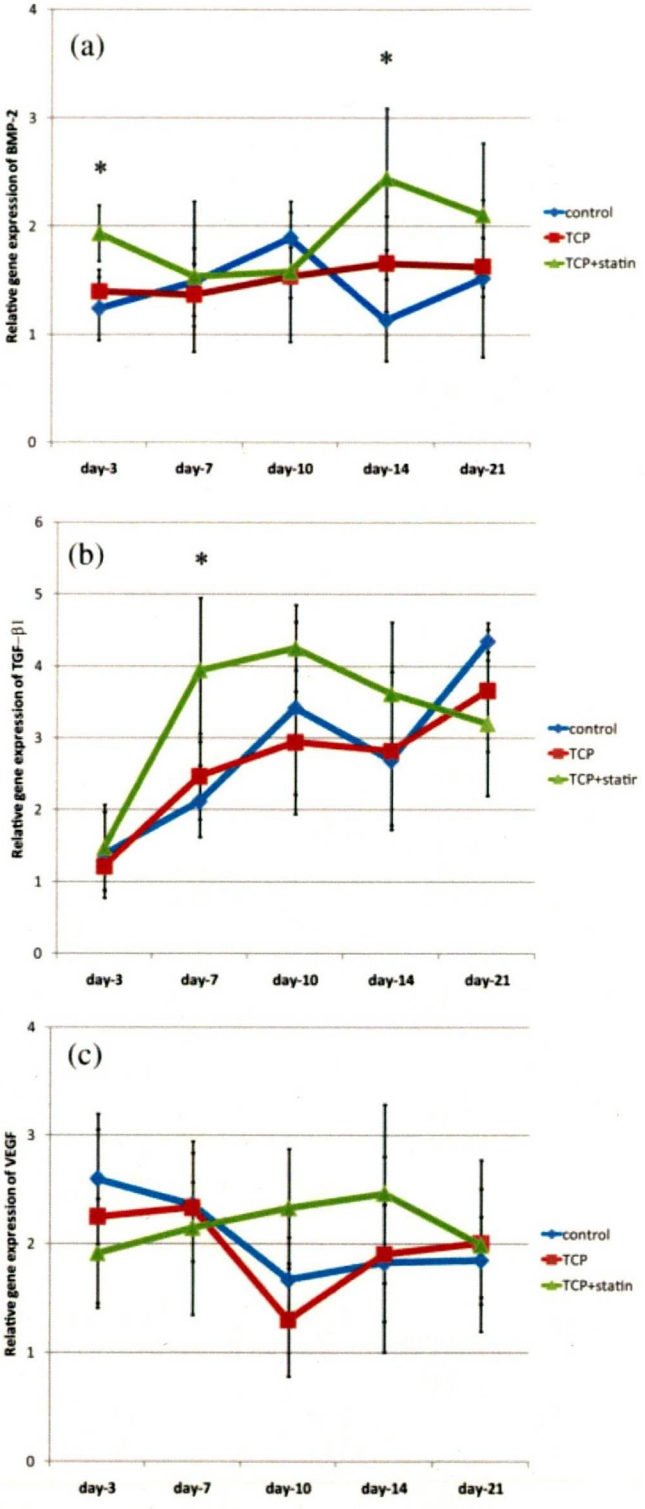

Figure 9. mRNA expression of (a) BMP-2, (b) TGF-β1 and (c) VEGF genes at different time points. Values were shown as mean ± SD, $n = 6$. *$p < 0.05$ compared with other groups at the same time point. [Color figure can be viewed in the online issue, which is available at www.interscience.wiley.com.]

group. This would contribute to increased differentiation of recruited osteogenic cells to osteoblasts and subsequently enhanced osteogenesis in the defect from day 14 to day 21. It is speculated that released simvastatin from resorbing αTCP stimulated the BMP-2 expression of osteogenic cells that were migrated from the dura mater and recruited around and inside αTCP particles at day 3. At later time points, auto- and paracrine upregulation of BMP-2 would play a role in continuing osteoblast differentiation and osteogenesis.

Maeda et al reported that statins augment vascular endothelial growth factor (VEGF) in osteoblastic cells *in vitro*.[32] In this animal study, VEGF was upregulated from day 7 to day 21 although the expression was not statistically different from control and TCP groups. Histologically, all groups revealed similar patterns of angiogenesis in the defect region.

Certain conditions must be considered when selecting an appropriate carrier or delivery system for drugs : (1) the ability of the system to deliver the drug at the appropriate time and in the proper dose, (2) the presence of a substratum that will enhance cell recruitment and attachment and will potentiate chemotaxis, (3) the presence of a void space to allow for cell migration and to promote angiogenesis, and (4) the ability of the delivery system to biodegrade without generating an immune or inflammatory response and without producing toxic waste products that would inhibit the repair process.[33] Alpha TCP used in this study fulfils all these requirements as a proper drug delivery system. It could release simvastatin sufficiently at the early time point when there is increased cellular proliferation and recruitment, thus augmenting the proliferation and recruitment of osteoprogenitor cells during this phase. Histological findings show that αTCP particles provided spaces into which osteogenic cells migrated and recruited. The particles also maintained spaces between them so that migrating osteogenic cells could be recruited and consequently differentiated and formed new bone whereas in control defects, middle of the bone defect was occupied by the connective tissue. Moreover, gradual dissolution of αTCP allowed a smooth exchange with newly formed bone without causing inflammatory response.

Although real-time PCR analysis indicated enhanced upregulation of BMP-2 and TGF-β1 mRNA expressions in simvastatin-αTCP combination group, it is not clear in which particular cell types these gene expressions were upregulated. Further studies using in-situ hybridization to detect the location of mRNAs would provide more information regarding the possible stimulatory effects of simvastatin on various cells in the bone defect. In addition, experiments to explore changes in the expression of other important genes such as FGF-2 and PDGF, which are also known to support cellular migration and proliferation, are also necessary for better understanding of the multiple effects of simvastatin in the molecular pathways that are involved in bone healing process.

In conclusion, within the limitation of this study, simvastatin combined with alpha tricalcium phosphate induced bone regeneration in rat calvarial defects by augmenting osteogenic cell proliferation, migration, recruitment and differentiation in the early phase of bone healing which were associated with increased expression of BMP-2 and TGF-β1.

REFERENCES

1. Einhorn TA. Clinical applications of recombinant human BMPs: Early experience and future development. J Bone Joint Surg Am 2003;85:82–88.
2. Mundy G, Garrett R, Harris S, Chan J, Chen D, Rossini G, Boyce B, Zhao M, Gutierrez G. Stimulation of bone formation in vitro and in rodents by statins. Science 1999;18:53–57.
3. Thylin MR, McConnell JC, Schmid MJ, Reckling RR, Ojha J, Bhattacharyya I, Marx DV, Reinhardt RA. Effects of statin gels on murine calvarial bone. J Periodontol 2002;73:1141–1148.
4. Wong RWK, Rabie ABM. Statin collagen grafts used to repair bone defects in the parietal bone of rabbits. Br J Oral Maxillofac Surg 2003;41:244–248.
5. Stein D, Lee Y, Schmid MJ, Killpack B, Genrich MA, Narayana N, Mark DB, Cullen DM, Reinhardt RA. Local simvastatin effects on mandibular bone growth and inflammation. J Periodontol 2005;76:1861–1870.
6. Sato D, Nishimura K, Ishioka T, Kondo H, Kuroda S, Kasugai S. Local application of simvastatin to rat incisor socket: Carrier-dependent effect on bone augmentation. J Oral Tissue Eng 2005;2:81–85.
7. Nyan M, Sato D, Oda M, Machida T, Kobayashi H, Nakamura T, Kasugai S. Bone formation with the combination of simvastatin and calcium sulfate in critical-sized rat calvarial defect. J Pharmacol Sci 2007;104:384–386.
8. Garrett IR, Gutierrez GE, Rossini G, Nyman J, McCluskey B, Flores A, Mundy GR. Locally delivered lovastatin nanoparticles enhance fracture healing in rats. J Orthop Res 2007;25:1351–1357.
9. Ozec I, Kilic E, Gumus C, Goze F. Effect of local simvastatin application on mandibular defects. J Craniofac Surg 2007;18:546–550.
10. Wang JW, Xu SW, Yang DS, Lv RK. Locally applied simvastatin promotes fracture healing in ovariectomized rat. Osteoporos Int 2007;18:1641–1650.
11. Wu Z, Liu C, Zang G, Sun H. The effect of simvastatin on remodeling of the alveolar bone following tooth extraction. Int J Oral Maxillofac Surg 2008;37:170–176.
12. Lee Y, Schmid MJ, Marx DB, Beatty MW, Cullen DM, Collins ME, Reinhardt RA. The effect of local simvastatin delivery strategies on mandibular bone formation in vivo. Biomaterials 2008;29:1940–1949.
13. Ma B, Clarke SA, Brooks RA, Rushton N. The effect of simvastatin on bone formation and ceramic resorption in a periimplant defect model. Acta Biomater 2008;4:149–155.
14. Moriyama Y, Ayukawa Y, Ogino Y, Atsuta I, Koyano K. Topical application of statin affects bone healing around implants. Clin Oral Impl Res 2008;19:600–605.
15. Jeon JH, Piepgrass WT, Lin YL, Thomas MV, Puleo DA. Localized intermittent delivery of simvastatin hydroxyacid stimulates bone formation in rats. J Periodontol 2008;79:1457–1464.
16. Ayukawa Y, Yasukawa E, Moriyama Y, Ogino Y, Wada H, Atsuta I, Koyano K. Local application of statin promotes

bone repair through the suppression of osteoclasts and the enhancement of osteoblasts at bone-healing sites in rats. Oral Surg Oral Med Oral Pathol Oral Radiol Endod 2008;107:336–342.
17. Nyan M, Sato D, Kihara H, Machida T, Ohya K, Kasugai S. Effects of the combination with alpha-tricalcium phosphate and simvastatin on bone regeneration. Clin Oral Impl Res 2009;20:280–287.
18. Einhorn TA. The cell and molecular biology of fracture healing. Clin Orthop 1998;355S:7–21.
19. Gerstenfeld LC, Cullinane DM, Barnes GL, Graves DT, Einhorn TA. Fracture healing as a post-natal developmental process: Molecular, spatial, and temporal aspects of its regulation. J Cell Biochem 2003;88:873–84.
20. Hobar PC, Masson JA, Wilson R, Zerwekh J. The importance of the dura in craniofacial surgery. Plast Reconstr Surg 1996;98:217–225.
21. Drake DB, Persing JA, Berman DE, Ogle RC. Calvarial deformity regeneration following subtotal craniectomy for craniosynostosis: A case report and theoretical implications. J Craniofac Surg 1993;4:85–89.
22. Opperman LA, Sweeney TM, Redmon J, Persing JA, Ogle RC. Tissue interactions with underlying dura mater inhibit osseous obliteration of developing cranial sutures. Dev Dyn 1993;198:312–322.
23. Gosain AK, Santoro TD, Song LS, Capel CC, Sudhakar PV, Madoub HS. Osteogenesis in calvarial defects: Contribution of the dura, the pericranium, and the surrounding bone in adult versus infant animals. Plast Reconstr Surg 2003;112:515–527.
24. Ogle RC, Tholpady SS, McGlynn KA, Ogle RA. Regulation of cranial suture morphogenesis. Cells Tissues Organs 2004;176:54–66.
25. Lind M, Eriksen EF, Bünger C. Bone morphogenetic protein-2 but not bone morphogenetic protein-4 and-6 stimulates chemotactic migration of human osteoblasts, human marrow osteoblasts, and U2-OS cells. Bone 1996;18:53–57.
26. Fiedler J, Röderer G, Günther KP, Brenner RE. BMP-2. BMP-4, and PDGF-bb stimulate chemotactic migration of primary human mesenchymal progenitor cells. J Cell Biochem 2002;87:305–12.
27. Lieberman JR, Daluiski A, Einhorn TA The role of growth factors in the repair of bone: Biology and clinical applications. J Bone Joint Surg Am 2002;84:1032–1044.
28. Marcelli C, Yates AJP, Mundy GR. In vivo effects of human recombinant transforming growth factor beta on bone turnover in normal mice. J Bone Miner Res 1990;5:1087–1096.
29. Noda M, Camilliere JJ. In vivo stimulation of bone formation by transforming growth factor-beta. Endocrinology 1989;124:2991–2994.
30. Lind M. Growth factor stimulation of bone healing. Effects on osteoblasts, osteotomies, and implants fixation. Acta Orthop Scand Suppl 1998;83:2–37.
31. Bruder SP, Fink DJ, Calpan AI. Mesenchymal stem cells in bone development, repair, and skeletal regeneration therapy. J Cell Biochem 1994;56:283–294.
32. Maeda T, Kawabe T, Horiuchi N. Statins augment vascular endothelial growth factor expression in osteoblastic cells via inhibition of protein prenylation. Endocrinology 2003;144:681–692.
33. Lieberman JR, Daluiski A, Stevenson S, Wu L, McAllister P, Lee YP, Kabo JM, Finerman GA, Berk AJ, Witte ON. The effect of regional gene therapy with bone morphogenetic protein-2-producing bone-marrow cells on the repair of segmental femoral defects in rats. J Bone Joint Surg Am 1999;81:905–917.

CLINICAL ORAL IMPLANTS RESEARCH

Kazuhiro Kon
Makoto Shiota
Maho Ozeki
Yasuo Yamashita
Shohei Kasugai

Bone augmentation ability of autogenous bone graft particles with different sizes: a histological and micro-computed tomography study

Authors' affiliations:
Kazuhiro Kon, Makoto Shiota, Maho Ozeki, Shohei Kasugai, Department of Oral Implantology and Regenerative Dental Medicine, Tokyo Medical and Dental University, Bunkyo-ku, Tokyo, Japan
Yasuo Yamashita, Department of Maxillofacial Anatomy, Tokyo Medical and Dental University, Bunkyo-ku, Tokyo, Japan

Correspondence to:
Kazuhiro Kon
Department of Oral Implantology and Regenerative Dental Medicine
Tokyo Medical and Dental University
1-5-45 Yushima
Bunkyo-ku
Tokyo 113-8549
Japan
Tel./Fax: +81 3 5803 5774
e-mail: k-kon.irm@tmd.ac.jp

Date:
Accepted 26 May 2009

To cite this article:
Kon K, Shiota M, Ozeki M, Yamashita Y, Kasugai S. Bone augmentation ability of autogenous bone graft particles with different sizes: a histological and micro-computed tomography study.
Clin. Oral Impl. Res. 20, 2009; 1240–1246.
doi: 10.1111/j.1600-0501.2009.01798.x

Key words: bone graft, dental implant, histology, micro-CT analysis

Abstract

Objectives: The purpose of this study was to investigate the augmentation process and ability of autogenous bone graft particles of two different sizes in a vertical augmentation chamber.

Material and methods: The cranial bones of 24 rabbits were used. Two polytetrafluoroethylene chambers were filled with harvested bone from tibia with small bone (SB; 150–400 μm) and large bone (LB; 1.0–2.0 mm) of the same weight. Animals were sacrificed after 1, 2, 4 and 8 weeks. The samples were analyzed by micro-computed tomography (micro-CT) for quantitative analysis, and embedded in polyester resin as non-decalcified specimens for histological analysis. Total bone volume (TBV), bone height (BH) and distribution of bone structure were calculated by micro-CT.

Results: Micro-CT evaluation and histology revealed a significant difference between the investigated specimens. TBV and BH of SB decreased to about 50% of the initial situation, and there was a statistically significant difference between 1 and 8 weeks. In contrast, TBV and BH of LB were almost retained at all experimental time points. Significant differences in TBV and BH were also observed between LB and SB at 8 weeks. Bone volume of SB decreased predominantly in the upper half of the chamber at 4 and 8 weeks. In the histological observations, SB showed favorable new bone formation and rapid bone resorption in a time-dependent manner during the entire experimental period. However, LB exhibited favorable morphological stability and continued new bone formation.

Conclusion: SB follows a smooth osteogenic process, whereas it is not effective in volume augmentation. LB is superior to SB in augmentation ability.

Oral implant therapy is now widely accepted as it provides a satisfactory esthetic and functional outcome (Ferrigno et al. 2002; Boronat-Lopez et al. 2009). To achieve these results, edentulous jaws should have adequate bone volume, which enables the placement of implants in an ideal position. In many cases, implant placement was restricted by bone resorption after teeth extraction, or the position of the mandibular canal and maxillary sinus. Therefore, bone augmentation is frequently planned in association with implant therapy (Lustmann & Lewinstein 1995; Chiapasco et al. 2004; Fugazzotto & Vlassis 2007; Hämmerle et al. 2008).

Currently, autogenous bone, allogeneic bone, xenogeneic bone and synthetic bone are being used as bone grafting materials (Moy et al. 1993; Yildirim et al. 2000; Rodriguez et al. 2003; Scabbia & Trombelli 2004; Turunen et al. 2004; Kihara et al. 2006). Among them, autogenous bone is widely regarded as the gold standard (Boyne

& James 1980; Moy et al. 1993]. However, autogenous bone grafts have several disadvantages, including morbidity of the donor site, limited amount of harvestable bone and ongoing volume reduction during the healing period. Especially, many researchers have demonstrated resorption of the grafted autogenous bone after surgery. Clinically, reduction of the buccal tissue volume was observed after autogenous block bone grafting in long-term follow-up studies (Widmark et al. 1997; Jemt & Lekholm 2003). The authors described this phenomenon as the result of grafted bone resorption. Moreover, autogenous bone grafted for maxillary sinus augmentation was reduced 6 months after surgery (Johansson et al. 2001).

The particle size of autogenous bone, which is considered to be one of the important factors that determine the augmentation ability, was studied in some articles (Zaner & Yukna 1984; Fucini et al. 1993; Springer et al. 2004; Murai et al. 2006; Coradazzi et al. 2007; Kuroki et al. 2008; Walsh et al. 2008). However, the conclusions of these investigations varied.

The purpose of this study was to investigate the augmentation process of autogenous bone graft particles of two different sizes in a vertical augmentation chamber and evaluate their augmentation ability.

Material and methods

Experimental protocols were approved by the Institutional Committee of Animal Care and Use at Tokyo Medical and Dental University. Japanese male white rabbits of weight (3.2–3.8 kg) and size were used (n = 24).

Surgical procedures

Animals were anesthetized preoperatively with an intramuscular injection of ketamine (50 mg/kg Ketalar, Sankyo, Tokyo, Japan) and thiopental sodium (25 mg/kg Rabonal, Tanabe, Tokyo, Japan). The surgical area was shaved and disinfected. In addition, 1.8 ml of a local anesthetic (2% xylocaine/epinephrine 1 : 80,000, Dentsply Sankin, Tokyo, Japan) was injected into the surgical sites before the start of surgery. Autogenous bone particles of two sizes were harvested from the tibia. The large particle bone (LB), which was cuboidal in shape (about 1 mm thickness and width with 2 mm length, standardized by sieves), was harvested with bone forceps. The small particle bone (SB), which was bone debris (150–400 μm diameter, average 250 μm), was harvested by a 3.2-mm-diameter trephine-bone-mill system (K-System, DentaK, Paris, France). Parietal bone was chosen as the augmentation model site. Skin incision and subperiosteal dissection were carried out sagittally between the parietal and the frontal bone, and the periosteum was raised. Polytetrafluoroethylene chambers (hollow cylinders with 5.0 mm inner diameter and 3.0 mm height having an outer brim) were fixed with stainless-steel screws (FKG Dentaire, Chaux-de-Fonds, Switzerland) to the parietal bone on the right and left sides. Bone of the same weight (60 mg) was grafted into each chamber with peripheral blood. The skin flaps were sutured with 3-0 silk. During the observation period, all rabbits were given water and a standard rabbit feed *ad libitum*. Rabbits were sacrificed at 1 week ($n = 6$), 2 weeks ($n = 6$), 4 weeks ($n = 6$) and 8 weeks ($n = 6$) with a lethal dose of thiopental sodium. The entire cranial bone was removed and fixed for 10 days in neutral 10% formalin.

Micro-computed tomography (micro-CT) analysis

Following the fixation period, grafted regions of specimens were quantified via micro-CT analysis (SMX-90CT, Shimadzu, Kyoto, Japan). Total bone volume (TBV) and bone height (BH) were calculated. TBV was acquired by the radiopaque voxels (cube 60 μm on one side) observed in the chamber. BH was evaluated from the distance between the basal host bone and the highest point of the bone fragment in the chamber and was measured in the center 3.0 mm diameter part of the chamber in each animal. The bone volume distribution in the upper and lower halves was also described as a percentile.

Histological processing

To obtain non-decalcified sections, cranial bone ($n = 24$) was dehydrated in ascending grades of ethanol, following fixation, and then embedded in polyester resin (Rigolac-70F, Rigolac-2004, Nisshin EM Co., Tokyo, Japan). These sections were cut (Exakt, Mesmer, Ost Einbeck, Germany) in the sagittal direction and ground to a thickness of about 300 μm. The sections were finally stained with 0.1% toluidine blue. Histological observation was performed under a light microscope.

Statistical analysis

To evaluate the influence of particle size on TBV and BH, intergroup data at each time point were statistically compared using the Kruskal–Wallis test and nonparametric multiple comparisons by Dunnet T3. Particle comparison within the same time point was analyzed using the Mann–Whitney test. *P*-values lt;0.05 were considered statistically significant. All statistical analyses were performed using a commercial computer program (SPSS 11.5, SPSS Inc., Chicago, IL, USA).

Results

Histology

SB-grafted sites

1 week. SB densely occupied almost the entire augmentation chamber and blood cells filled the inter-SB space. SB, which stained strongly with toluidine blue, retained its original chip-like shape. No osteoclast- or osteoblast-like cells were observed at this stage (Fig. 1a and b).

2 weeks. SB occupied nearly entire the chamber as in the first week, and the height of SB did not change (Fig. 2a). At the lower part of the chamber, numerous multinuclear giant cells were observed on the surface of SB, newly formed bone was partially observed on the surface of grafted bone and large amounts of fibrous connective tissue were observed in the interspace of the graft. Especially, in the region close to host bone, new blood vessels had formed. However, at the upper part of the chamber, there was no new bone formation; instead, part of the SB had undergone resorption by multi nuclear giant cells (Fig. 2c).

4 weeks. Bone area that exhibited constricted bone trabeculae occupied about half or more of the height of the chamber. Grafted SB had resorbed mostly in the upper part (Fig. 3a). Loose fibrous connective tissue was observed in the upper half of the chamber, and some fibrous connective tissue ran in a direction parallel to the bone

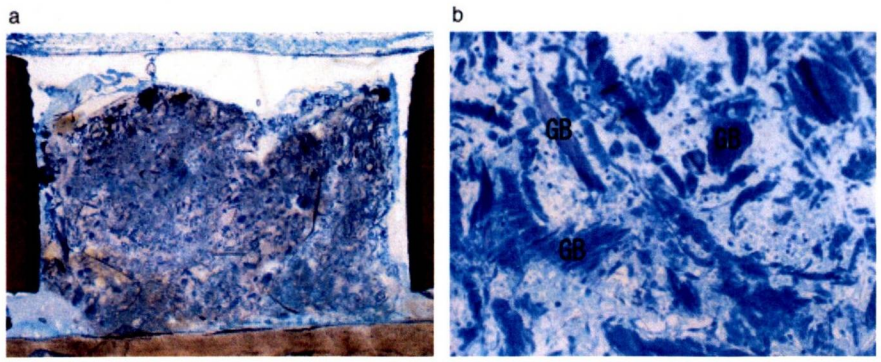

Fig. 1. Small bone grafted site at 1 week. (a) Grafted bone (GB) was observed over the entire augmentation chamber. GB retained its original chip-like shape. However, no newly formed bone was observed. Magnification × 2.5. (b) High-magnification image of (a). GB was strongly stained with toluidine blue. The interparticular space was occupied by blood cells. Magnification × 50.

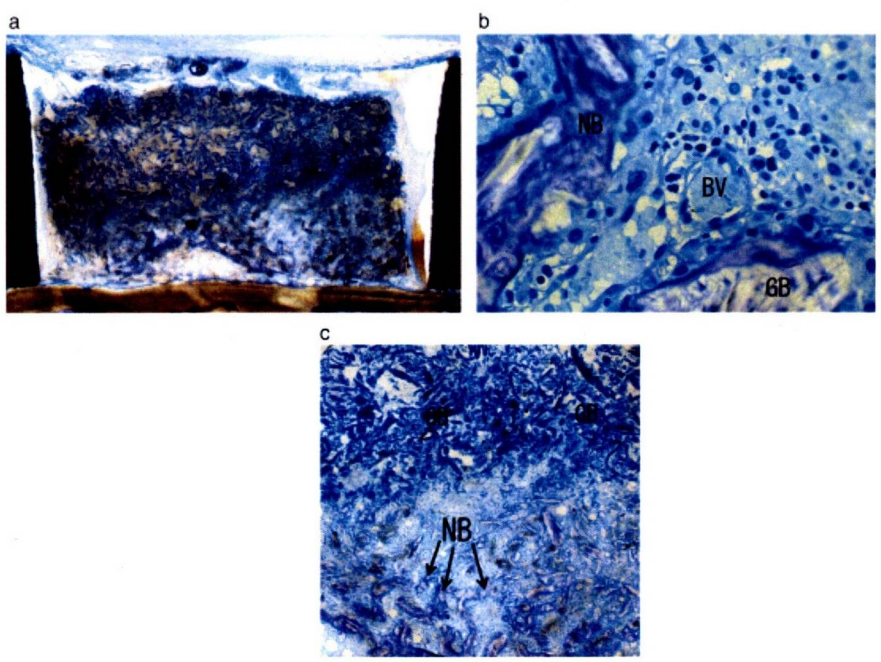

Fig. 2. Small bone grafted site at 2 weeks. (a) Grafted bone (GB) occupied the the entire chamber same as the 1-week model. The GB height was almost preserved. Magnification × 2.5. (b) High-magnification image of (a). New bone formation was observed from the region close to the host bone surface toward the GB. Blood vessels (BV) were also observed. Magnification × 100. (c) In the lower part of the chamber, near the host bone, newly formed bone (NB) was observed on the GB surface. In the upper part of the chamber, there was no new bone formation; instead, a part of GB underwent resorption by a multinuclear giant cell. Magnification × 10.

area. At higher magnification, grafted SB was mostly resorbed and replaced by newly formed bone. Mature blood vessels were observed in the interspace of the bone structure, and many fat cells were observed around the host bone (Fig. 3b).

8 weeks. The height of bone area was about a quarter of the chamber and the number of trabeculae had reduced when compared with the 4-week specimens. Loose fibrous connective tissue was observed in the upper region of the chamber. A large number of fat cells were observed over the entire chamber (Fig. 4a). Grafted bone was almost completely replaced by new bone that was surrounded by blood vessels and fat cells. Osteoclast-like cells were observed in the resorption lacunae within newly formed bone (Fig. 4b).

LB-graft sites

1 week. LB occupied a large part of the chamber. LB stained less with toluidine blue and resorption lacuna were not detected on the surface of grafted bone at this time point (Fig. 5a). In the interspace of grafted bone, very loose fibrous connective tissue and a few blood vessels were observed (Fig. 5b).

2 weeks. LB preserved its original block-like shape and low stainability. The height and space of the bone structure was maintained. The interspace of the grafted bone was filled with fibrous connective tissue (Fig. 6a). A few osteoclast-like cells were observed on the grafted bone. In the vicinity of the host bone, moderately mature blood vessels were found, and new bone had formed from the host bone surface toward the grafted bone (Fig. 6b).

4 weeks. LB was positioned at a higher level in the chamber and it retained its original form and low stainability (Fig. 7a). However, new bone formation was observed from the host bone surface to the grafted bone surface and Howship's lacunae with many osteoclast-like cells were found on the surface of the grafted bone in the upper part of the chamber (Fig. 7b). Fibrous connective tissue and blood vessels were observed around the grafted bone, and fat cells were detected around the host bone surface.

8 weeks. LB was only modestly integrated with newly formed bone that had high stainability, and the graft stained slightly stronger than at 4 weeks. Many osteocyte-like cells were observed on the grafted bone and a few osteoclast-like cells were also detected in the resorption lacunae (Fig. 8a). Around this bone architecture, numerous blood vessels were observed (Fig. 8b). There were many fat cells over the entire chamber, especially, near the host bone surface.

Micro-CT analysis

Radiological quantitative analysis was performed by micro-CT (Fig. 9)

Intergroup comparisons. TBV showed significant differences for 1 week/8 weeks in the SB group ($P = 0.026$), and 2/4 weeks in the LB group ($P = 0.025$). BH showed significant differences for 1 week/4 weeks ($P < 0.001$), 1 week/8 weeks ($P < 0.001$), 2/4 weeks ($P < 0.001$) and 2/8 weeks ($P < 0.001$) in the SB group. No other significant differences were found (Fig. 10a and b).

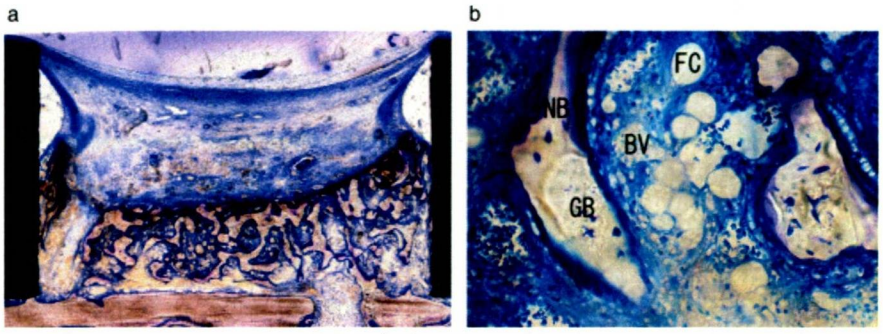

Fig. 3. Small bone grafted site at 4 weeks. (a) Newly formed bone (NB) occupied about half or more the height of the chamber. NB constricted bone trabeculae. Magnification × 2.5. (b) High-magnification image of (a). NB was observed around the grafted bone (GB). Mature blood vessels (BV) and fat cells (FC) were also observed in the interspace of the bone structure. Magnification × 50.

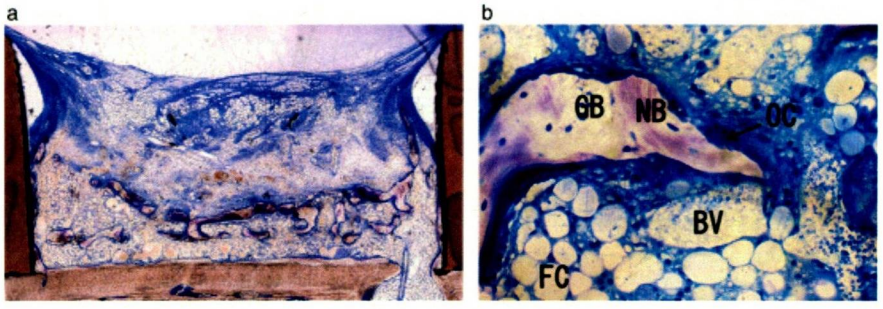

Fig. 4. Small bone grafted site at 8 weeks. (a) Accelerated bone resorption was observed in the 8-week model. A large number of fat cells were observed over the entire chamber. Magnification × 2.5. (b) High-magnification image of (a). Mature blood vessels (BV) were observed around the newly formed bone (NB). Grafted bone (GB) was almost completely replaced by new bone. An osteoclast-like cell (OC) was observed in the NB. Magnification × 100. FC, fat cell.

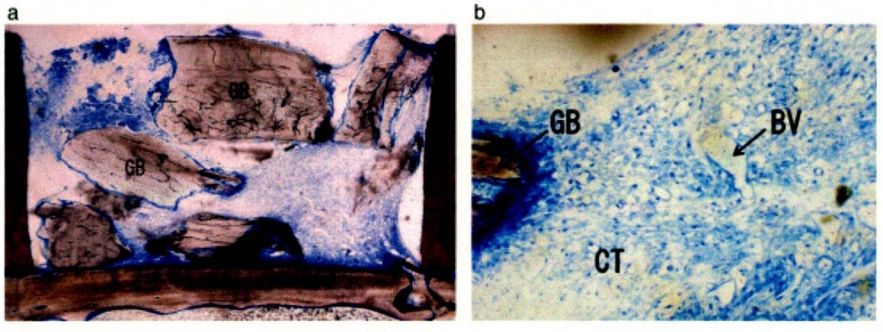

Fig. 5. Large bone grafted site at 1 week. (a) Grafted bone (GB) was observed over the entire chamber. Bone resorption was not observed around the surface of GB at this time point. Magnification × 2.5. (b) High-magnification image of (a). In the interspace of the GB, there was very loose fibrous connective tissue (CT), and a few blood vessels (BV) were also observed. Magnification × 25.

SB vs. LB

TBV and BH showed notable significant differences at 4 weeks (TBV: $P = 0.004$, BH: $P = 0.002$) and 8 weeks (TBV: $P = 0.006$, BH: $P = 0.004$). At 1 week and 2 weeks, there was no significant difference (Fig. 10a and b).

Distribution of bone structure

LB groups exhibited no remarkable changes. In contrast, bone volume reduction of the upper half was prominent in the 4- and 8-weeks of SB groups (Fig. 10c).

Discussion

Autogenous bone has long been considered the most excellent material for bone augmentation (Boyne & James 1980; Moy et al. 1993). However, it was recently reported that autogenous bone grafts showed continuous volume reduction during the healing and follow-up periods. During maxillary sinus augmentation, the volume of autogenous grafts was reduced to 49.5% of the initial volume after 6 months (Johansson et al. 2001). In addition, it was demonstrated that the surgically augmented height with an autogenous block graft decreased to 60% after 10 months (Widmark et al. 1997).

The particle size of graft material has been regarded as one of the major factors that determine the ability of augmentation, and it has been studied by many researchers. However, these studies have reported variable conclusions so far. The aim of this study was to investigate the augmentation process and the ability of autogenous bone graft particles of two different sizes.

In the present study, TBV of the SB group decreased in a time-dependent manner; it decreased to 51.3% of the initial volume. Histological analysis showed that the grafted bone in the lower half had resorbed by multinuclear giant cells at 2 weeks, and was partially replaced by newly formed bone at 4 weeks. A great deal of newly formed bone had resorbed at 8 weeks. Thus, SB groups were considered to follow the remodeling process. In the upper part of the chamber, strongly stained SB observed at 2 weeks had resorbed by 4 weeks. This resorption caused volume reduction between 2 and 4 weeks. On the other hand, TBV of the LB group exhibited a volume increase at 4 weeks, and it was almost maintained at 8 weeks. Histologically, LB almost preserved its shape at 2 weeks and new bone formation was observed from the host bone to the LB surface at 4 weeks. The formation and resorption of bone was observed at 8 weeks. In addition, in the 4-week LB group, the original grafted bone of the upper half had the same low stainability, although numerous osteoclast-like cells were observed on the surface of the grafted bone. A greater part of the original grafted bone was maintained in the LB-grafted site at 8 weeks; meanwhile, the original grafted bone almost disappeared in the SB groups. This behavior of bone remodeling was thought to cause the difference in TBV between LB and SB.

The larger particle size of the grafting material was more beneficial than the small size bone grafts in augmentation. Demineralized freeze-dried bone allografts